RSC Advances

ROYAL SOCIETY OF CHEMISTRY

www.rsc.org/advances

Hydrothermal Synthesis and Electrochromism of WO_3 Nanocuboids

Sangeeta Adhikari and Debasish Sarkar[#]

Department of Ceramic Engineering, National Institute of Technology, Rourkela, INDIA

Abstract

Tungsten trioxide (WO_3) nanocuboids preferentially develop through control over three important processing parameters; fluoroboric acid concentration, hydrothermal reaction time and temperature. Fluoroboric acid concentration has significant influence on conversion of phase transformation from triclinic to monoclinic followed by intermediate metastable hexagonal tungsten trioxide and simultaneous formation of thin plate to cuboid shape. An optimum temperature and time is essential to achieve cuboid morphology without content of any crystalline water molecule. Orthorhombic tungstite (H_2WO_4) grows from virgin precursors below 180^oC temperature prior to the formation of triclinic WO_3. Monoclinic nanocuboid has average dimension of length ~ 140nm, width ~ 120nm and thickness ~ 85nm, but reduces their surface area and enhances the crystallinity beyond an optimum time of duration. The probable hydrothermal assisted reaction has been proposed to justify the formation of morphology and selective phase. Band gap energy of WO_3 insignificantly vary with respect to processing conditions, lowest is 2.75ev.The current density 3.15mA/cm^2 is attributed to high symmetry electrochemical reaction of dip-coated nanocuboid WO_3/ITO electrode. Coloration and bleaching kinetic depicts the proton assisted bleaching is faster than the coloration phenomenon in appearance of ~72.2% electrochromic reversibility. The fabricated nanocuboid WO_3coated ITO glass has fairly good optical transparency, electrochromic stability and reversibility.

Key Words: Tungsten Trioxide, Hydrothermal, Nanocuboid, Band gap energy, Electrochromism.

[#]Corresponding Author: Debasish Sarkar (dsarkar@nitrkl.ac.in), Tel: 06612462207.

1. Introduction

Tungsten trioxide (WO_3), an n-type semiconductor has been renewing attention in recent times due to its intriguing physicochemical properties [1]. Nanostructured oxide semiconductor is of considerable interest because of their potential applications in devices such as gas sensors, solar cells, and photocatalysts [2].Its property is not limited to electronic and optoelectronic devices but also applicable for condensed matter physics to solid state chemistry.The oxide nanoparticles with different morphologies, in particular, have held much concern due to their distinctive physical and chemical properties, which depends on their morphology and crystal structure [3, 4]. Morphology management is a challenging task for the investigation of their application potentiality. Moreover, lessen metal oxide dimension enhances the electrical and optical performance to tune the modern device properties. The complex three-dimensional (3D) nanostructures have attracted much attention since this nanostructure possesses features of nanometer-scaled building blocks and novel properties [3]. In general, cuboid morphology has high surface area and consequent surface energy over spherical shape[5]. Thus, control over the morphology of semiconductor materials is a critical issue and fascinating research area.Over the past few decades, the tungsten oxide semiconductor material has been extensively studied due to their high coloration efficiency and good cyclic stability among various electrochromic materials. Extensive literature review suggests that the different morphologies of WO_3in nanometer scale have already been prepared for the functionality of nanomaterial and electrochromic devices [6-7]. Most of the morphology has been achieved by different solution based methods like sol-gel, co-precipitation, hydrothermal and numerous vapor-phase deposition methods [8-10]. Hydrothermal method is one of the economic wet chemical routes over physical deposition techniques to prepare different morphologies of nano-structured WO_3 in presence of structure-directing agents like acids, surfactants and metal sulphates, chlorides and sulphides [11-13]. Recently, fluoroboric acid (HBF_4) has also been used to synthesize nanoplates and designated as a structure directing agent [1].

A comparative study demonstrates that the orthorhombic WO_3 rectangular slab, nanowire and nanorod have been synthesized by using structure directing agents for the photodecomposition of Procion Red MX-5B dye [14]. In another process,Su et al. synthesized both uniform orthorhombic and monoclinic WO_3 square nanoplates with the assistance of tartaric and citric acid by hydrothermal process, respectively [15].An aqueous sol transforms to $WO_3.2H_2O$ gel through an ion exchange method which develops plate shaped WO_3 after screen printing for NO_2 sensing [16].Another research group studies the synthesis of tungsten oxide nanoplates from tungsten (VI) ethoxide under low temperature with supercritical water in a continuous flow system. Rietveld refinement confirms the presence of 93% hexagonal crystal structure and 7% triclinic structure of the WO_3 nanoplates.The flow rates andPEG as surface modulator plays an important role to control the ultimate morphology [17]. A crystal seed assisted hydrothermal method has also been employed to assemble plate and brick like nanostructured $3WO_3.H_2O$ films directly on FTO glass substrate through Na_2SO_4 as the capping agent. However, nanoplate exhibits relatively higher current density of $0.2mA/cm^2$ than partially crystalline water containing nanobrick films for both intercalation/deintercalation processes over the same period [18].Another comparative study demonstrates that the capping agents Na_2SO_4, $(NH_4)_2SO_4$ and CH_3COONH_4 for oxidation of methanol and water splitting has the significant effect on the formation of plate, wedge and sheet-like orthorhombic WO_3 nanostructures. The highest photoconversion efficiency of 0.3% is observed for sheet-like WO_3 prepared using CH_3COONH_4under simulated solar illumination [19]. A highly porous thick and opaque WO_3 films fabricated by sol gel method exhibits a similar reversible electrochromic property for 1^{st} and 1000^{th} cycle of cyclic voltammograms in 1M $LiClO_4$with $0.2mA/cm^2$as current density [20]. A low cost hydrothermal approach has been done to prepare thick plate like monoclinic tungsten oxide nanostructured film onto FTO glass substrates for the estimation of electrochemical properties for electrochromic display windows application [21].The process temperature variation or annealing under different condition leads to the formation of different crystal structures, in which monoclinic spherical morphology demonstrates a high degree of

photocatalytic activity for oxygen evolution through water splitting in comparison with the orthorhombic phase[22].There have been many reports on the synthesis of various two dimensional plate shaped particles but limited literature report are found on three-dimensional nanostructures other than spherical morphology which encourages concentrating on this particular morphology. The techniques such as Langmuir Blodgett technique, dip coating and sputtering technique have been used for the assembly of nanomaterials. These require complicated operating procedure and specific equipments with addition of certain surfactants [23-25]. Although, literature recommends hydrothermal coating as one of the methods for thin film fabrication, but a low-cost method for large scale fabrication of tungsten oxide nanostructures is still lacking.In this context, we have synthesized three dimensional monoclinic nanocuboids of WO_3 through hydrothermal method and characterized them in terms of pure-phase crystal structure, surface area and morphology. A plausible reaction process had also been suggested and optimized the critical processing parameters to control the monoclinic cuboid structure of WO_3. Furthermore, electrical and optical properties of optimized WO_3nanocuboids have been carried out to justify the electrochromic effect of dip-coated WO_3/ITO electrode.

2. Experimental Procedure

2.1. Preparation of WO_3 Nanocuboids

Sodium tungstate ($Na_2WO_4.2H_2O$) was used as base precursor along with fluoroboric acid as structure direct agent to synthesizeWO_3 nanocuboids. Prior to hydrothermal treatment,the fluoroboric acid (HBF_4, 50% w/w) solution was added to sodium tungstate aqueous solution and constantly stirred on a magnetic stirrer at 300rpm for 30 minutes which transformed to yellowish green precipitate. The solution together with the precipitate was then transferred to a 50ml Teflon beaker, placed inside an autoclave (high pressure metal bomb), which was sealed tightly and kept at certain temperature for a predetermined time in a hot air oven. After autoclaving, the precipitate together with the solvent was

centrifuged at 13000rpm to remove the excess HBF_4.Hot water followed by isopropanol was used for washing of the precipitate. The residue after centrifuging was freeze dried at a temperature of -52^oC and a vacuum of 10torr. Solute concentration and effective volume of the reaction chamber were also important considerations for the aforementioned process. The experiments were carried out by varying the concentration of HBF_4, time duration and reaction temperature to optimize the crystal structure and morphology. A series of experiments were conducted at various solute concentration, constant temperature 180^oC and constant time 4hours.Similarly, additional experiments were carried to understand the effect of hydrothermal duration and temperature.The powders were characterized in terms of crystallinity, crystal structure, and morphology by different physicochemical techniques.

2.2 Characterization of WO_3Nanocuboids

X-ray diffraction (XRD) patterns for the powders were obtained using a Philips X-Ray diffractometer with Ni filtered CuK_α radiation (λ= 1.5418 Å).Rietveld refinement of the optimized data was analyzed using 'fullprof suite' program and compared with the PCR database. Differential scanning calorimetry and thermogravimetric analysis (DSC– TG) of WO_3 nanocuboids after synthesis for 4hours and 6hours was carried out using Netzsch, Germany, STA449C/4/MFC/G apparatus. FESEM images for hydrothermally treated samples were carried out to understand the morphological changes with respect toHBF_4concentration, duration and temperature variation using NOVA NANOSEM FEI450 system.For this, the samples were mounted on a double sided carbon tape attached to SEM stub and sputter coated with gold for 120 seconds. Specific surface area of the powders was measured using nitrogen as the adsorbate in a BET apparatus (QuantachromeAutosorb, USA). Morphology of WO_3nanocuboids was further studied by transmission electron microscope (JEOL JEM-2100).Diffuse reflectance measurement was done through Shimadzu spectrophotometer (UV-2450) to evaluate band gap energy for WO_3 nanocuboids. Room temperature diffuse reflection percentage was measured in the wavelength region 200 – 700nm.

2.3 Fabrication and electrochemical measurement of WO_3 coated ITO

WO_3nanocuboid particles were homogeneously dispersed in ethanol,and dip-coated onto a transparent conducting oxide (TCO) substrate to evaluate the electrochromic effect of WO_3/ITO electrode having $2cm^2$ area (dimensions: 2cm x 1cm). The stable WO_3suspension was prepared by ultrasonication of solution containing 0.5 gm of WO_3 nanopowders in 4ml absolute ethanol. Commercial grade 84% optically transparent conducting Sn-doped Indium oxide (ITO) glass substrate was used as the TCO substrate to fabricate the working electrode. Conductive ITO glass substrate was cleaned by ultrasonication through a successive immersion in distilled water, acetone and ethanol prior to WO_3 coating. The dip coated samples was dried at 60^oC for 30 min [26]. The electrochemical properties for WO_3/ITO electrode were determined by Cyclic Voltammetry (CV), Chronoamperometry (CA) and Chronocoulometry (CC) techniques. The direct optical transmittance was also measured using UV-Vis spectrophotometer using bare ITO glass substrate as a reference electrode.The electrochemical intercalation and deintercalation of electrons and H^+ ions was carried out using Biologic Science Instruments SP-50 controlled by a personal computer having EC-lab software in the three electrode cell configuration using 1M H_2SO_4 electrolyte solution with Platinum (Pt) as a counter electrode, saturated Ag/AgCl as a reference electrode and as prepared WO_3films as the working electrode.

3. Results and Discussion

3.1. Influence of processing conditions

Powder diffraction pattern confirms the phase content, crystal structure and crystallinity of WO_3 nanopowders. The room temperature XRD pattern for all the powders has been shown in Figure 1. Initially, designing of experiments is concentrated to know the primary crystal structure and phase of the products formed on changing the HBF_4molar concentration (M) from stoichiometric 2M to the higher concentration of 5M. The other parameters are kept constant such as temperature 180^oC and

time 4hours during this experiment.The XRD pattern of synthesized powders under these conditions has been shown in Figure 1a.ThestoichiometricHBF_4concentration (2M) begins to form triclinic tungsten oxide phase mixed with partial monoclinic phase (JCPDS Card No-830949 and 431035).Pure triclinic tungsten oxide (JCPDS Card No- 830949) phase is recorded with increasing concentration of 2.5M HBF_4. There are no peaks of a monoclinic phase found in this concentration. A pure hexagonal tungsten oxide phase (JCPDS Card No-752187)is starting to form at 3M HBF_4 concentration.In the later stage, coexistence of hexagonal and monoclinic phase is found for 3.5M concentration.This depicts the plausible conversion of hexagonal to monoclinic phase. Pure monoclinic crystalline tungsten oxide (JCPDS Card No- 720677) phase is observed upon further increasing the concentration (4M to 5M) as shown in the figure.The above investigation shows that WO_3 transition follows triclinic to hexagonal followed by monoclinic as similar observation revealed by Zadeh et al [1, 27]. Both stable triclinic and monoclinic WO_3 phases are formed by varying the HBF_4 concentration in the present studied system.However, hexagonal phase occurs as only a metastable phase which has a tendency to form stable monoclinic phase with further HBF_4 concentration increment; preferably beyond 4M [28].

Growth phenomenon depends on the time under isothermal condition irrespective of any process condition [29]. Hence, it is necessary to understand the time effect on the formation of pure phase along with desired morphology. A time variation is done starting from 0 – 8hourswhile keeping other parameters constant such as 4M HBF_4 concentration and temperature 180^{o}C as shown in Figure 1b.The choice of molar concentration of $HBF_4$is 4M as after this concentration; it favors to form monoclinic phase only. Zero hour has been defined as before insertion of the closed vessel in hydrothermal process chamber. ImmediateHBF_4addition results in orthorhombic tungstic acid (Tungstite, JCPDS Card No- 840886) along with some impurity peaks. Pure orthorhombic tungstite (Tungstite, JCPDS Card No- 840886) phase is only formed at 2hours duration.Interestingly, the crystalline monoclinic phase has been detected for the duration of 4hours and phase remains constant

beyond this time limit. The result depicts the periodic formation of orthorhombic tungstite (H_2WO_4) and monoclinic WO_3crystal structures by varying the hydrothermal duration. Process control variables suggest that the optimized condition to obtain pure monoclinic tungsten oxide is 4M HBF_4 concentration, 4hours duration and 180^oC temperature. However, this condition provides low crystalline cuboid morphology and subsequent band gap energy due to content of crystalline water [30]. The presence of water content phenomenon is further confirmed by thermal analysis in the next section. In this consequence, six hours processing time is again considered as the optimum hydrothermal time. However, no significant change in the crystallinity is observed after hydrothermal duration of 6hours.Every synthesis requires a minimum thermal energy to overcome the potential energy barrier for the completion of the targeted reaction. To optimize this, additional study on varying the reaction temperature (160^oC to 200^oC) has also been carried out at constant conditions such as 4M HBF_4concentrationand 6hoursreactionduration. Figure 1c clearly represents the orthorhombic tungstic acid at 160^oC. But, a mixture of orthorhombic tungstic acid and monoclinic tungsten oxide is resulted at 170^oC, which indicates the initialization of monoclinic crystal phase at such temperature. Additionally, the increment temperature upto 200^oC only enhances the crystallinity of a monoclinic phase or in other sense decreases the surface area. Thus, an optimized condition for the synthesis of WO_3 nanocuboids from $Na_2WO_4.2H_2O$ and HBF_4 is temperature 180^oC, time 6hours and 4M HBF_4 concentration.

3.2. Rietveld refinement for optimum WO_3Nanocuboids

In a recent article, Ma et al.[1] has started from aforesaid precursors and reports an identical XRD pattern up to a maximum 2θvalue of50^{o}andconcluded the structure to be triclinic as per JCPDS – 321395. In comparison, the present XRD pattern for extended diffraction angle 15-80^o (2θ) consists broader peaks at higher angles of 53 – 57^o (2θ). This peak in particular well matches with monoclinic instead of triclinic tungsten oxide crystal structure as confirmed from Rietveld profile fitting method

(Figure. 2). Tungsten oxide is calculated aspure monoclinic structure (PCR file code: wo3_p21n_80056, a = 7.39773, b = 7.49056, c = 7.64700, β= 88.7102°with space group: P21/n). The crystal structure model of WO_3(PCR file code: 80056) is used as a starting point for the refinement.The characteristic reflections of WO_3 are pointed as (200), (020) and (002). It is observed that reflections are merged into a broader peak centered at the (020) position, which may be due to the overlap of the strongly broadened peaks. The Rietveld refinement havelowest indices valueswhich are recorded as R_p = 23.2,R_{wp} = 29.9 and χ^2 = 1.34, respectively [31].

3.3. Thermal analysis of WO_3Nanocuboids

Thermal analysis of WO_3nanocuboidsfor both4hours and 6hourshas been presented in Figure 3a and Figure 3b, respectively. The thermogram of 4hours illustrates the instability of the compound till 280°C. A total of 3.5% weight loss is observed from room temperature to 280°C which corresponds to the presence of water molecules in the WO_3nanocuboidcrystal system.In DSC plot, the endothermic peak near to 80°C corresponds to the loss of physisorbed water. A broad exothermic peak at around 550°C is associated with the further crystallization of WO_3. But, the thermogram of 6hoursrevealshigh thermal stability of the compound till 600°C as there is no weight loss, but plausible crystallization at high temperature has been depicted by a small exothermic hump.This study predicts the synthesized particles have a tendency to the high degree of crystallinity at high temperature; as the powder synthesized at low temperature has a tendency to form semi-crystalline structure [32].Phase changes of specific cuboid WO_3 morphology during hydrothermal reaction follows orthorhombic tungstite → monoclinic WO_3 transformation, which has already been confirmed through crystal phase and thermal analysis at optimum HBF_4 molar concentration. The aforementioned process conversion can be represented through Equation 1 – 3.

$$Na_2WO_4.2H_2O + 2HBF_4 \longrightarrow H_2WO_4(\text{orthorhombic}) + 2NaBF_4 + 2H_2O \quad (1)$$

$$H_2WO_4\ (\text{orthorhombic}) \longrightarrow WO_3.xH_2O(\text{monoclinic}) + H_2O \quad (2)$$

$WO_3.xH_2O \longrightarrow WO_3 + xH_2O$ (3)

The value of 'x' is found as0.5and confirmed from the thermogravimetric data presented in Figure. 3.

3.4. Morphological analysis of WO_3Nanocuboids

The reaction sequence, concentration of HBF_4, temperature and time are encountered to illustrate different morphologies and represent their FESEM images in Figure 4-6. Discrete small dots appear due to gold coating. Detail analysis suggests that the 4M HBF_4 concentration develops adequate crystal structure, crystallinity and desired morphology. Hence, lower and upper limits such as 3.5M and 4.5M HBF_4 concentration have been considered for fine tuning and details understanding. Figure 4arepresents three particles prepared at 3.5M, 4M and 4.5M HBF_4 concentrations, respectively. Low concentration prefers to form partially agglomerated spherical particles along with plate shaped particles instead of any nanocuboids. But, the optimum at 4M concentration forms nanocuboid morphology as shown in Figure 4b.Typical dimension of cuboid appears to be of length ~ 130nm, width ~ 110nm and thickness ~ 85nm from the image. However, further concentration increment has no distinct influence on the morphology as described in Figure 4c. Figure 5 shows the effect of the hydrothermal duration on the morphology of $WO_3$and the plot of specific surface area vs. time to understand the growth phenomenon affecting by the surface activity.Hydrothermal duration of 2hours initially develops uniform plate like morphology with average particle size of 400nm and orthorhombic tungstite crystal structure.Herein the selected hydrothermal method follows development of expected WO_3 crystal from aqueous metal salt solutions under critical pressure at a pertinent temperature and solution pH through the structure directing agents. The WO_3nanoparticle formation mechanism with particular growth direction depends on the solubility of the metal oxides and the reaction kinetics during the synthesis. It significantly alters the critical point when temperature assists to form high pressure and changes the resultant dielectric properties of aqueous media [33]. At the initial stage, tungstite (H_2WO_4) formation occurs whose structure has layers of WO_6 octahedra sharing

four equatorial oxygen atoms which are linked through hydrogen bonds derived from interaction between water molecules and oxygen present in the axial position of the octahedral. Plate shaped particle is formed due to inhibition of the (010) crystal plane which is the normal growth direction of H_2WO_4 structure [1]. Due to insufficient BF_4^- anion concentration, structural orientation of plates cannot be induced by adding BF_4^- anion to the hydrogen bond system to occupy the apexes with a boron atom at center. Thus, the growth axis is not restricted rather prefers growth of the structure forming cuboids. Moreover, further time increment up to 4hours; the cuboid like WO_3particles is mixed with a fraction of the plate like particles. This reveals that the growth mechanism follows a plate to cuboid like morphology. Almost homogeneous cuboid like morphology has been observed for 6hours without formation of any plates. A gradual decrement surface area is observed with the time increment because of agglomeration of particles. It reveals that due to high active surface, the particles tend to stabilize themselves following the agglomeration process. Figure 6 represents the effect of lower and upper temperature range from critical temperature 180^{o}C. Plate like particles and more agglomerated cuboid like particles are confirmed at 170^{o}C and 190^{o}C temperature, respectively. Figure 7 represents the TEM micrograph including HRTEM image and SAED pattern for WO_3 nanocuboids. Figure 7a shows soft agglomerated distinct nanocuboid morphology of WO_3 nanoparticles with an average particle length ~ 140nm and width ~ 120nm. Topographical feature seems that the particle edges are imperfect and attribute to the effect of certain tilting angle of individual cuboid particles, whereas TEM of plate morphology exhibits perfect edges as reported by Su et al [15]. Figure 7b represents the HR-TEM image of a single nanocuboid. The image clearly shows the resolved lattice fringes in the visible range, indicating its single crystalline nature. The lattice distance is found to be 0.36nm which can be readily indexed to (002) plane of monoclinic WO_3 nanocuboids. The value calculated also resembles the value calculated from the X-RAY diffraction pattern which indicates the tentative growth of the particle along this crystal plane. Figure 7c shows the Selected Area Electron Diffraction (SAED) pattern of a single crystalline WO_3 nanocuboid. In general, the h = 0, k = 0 and l =

x (where x = 1, 2 or 4) plane restrict the 3D growth pattern and develop 2D plate shaped morphology [34]. However, the TEM illustration depicts that the high crystalline WO_3 exhibits excellent growth phenomenon along the [002] direction to form cuboid morphology.

3.5. Band Gap of WO_3Nanocuboids

Band gap energy of the selected powder is measured from the UV-Vis diffuse reflectance spectra. The measured diffuse reflectance spectra (Figure 8) has been used for the estimation of band gap energy from Tauc plot, which is the square root of Kubelka – Munk function multiplied by the photon energy and plotted against the photon energy ($E_{photon} = h\lambda$) as shown an inset of the Figure 8.The Kubelka – Munk unit of absorption is calculated from the following equation;

$KMU = (1 - R)^2/2R$, where, R = reflectance [10]. Band gap energy is calculated after synthesis at different conditions. For e.g; 2M HBF_4 concentration at 180^{o}C for 4hours with triclinic WO_3 structure; 3M HBF_4 concentrations at 180^{o}C for 4hours with hexagonal WO_3 structure; 4M HBF_4 concentrations at 180^{o}C for both 4hours and 6hours with monoclinic WO_3 structure are considered for the band gap measurements. The band gap energy of triclinic and hexagonal crystal structures is calculated to be 3.25eV and 2.85eV, respectively as illustrated as 3.09eV for hexagonal structure in previous report [11].Near to equal range of band gap energy 2.75eV is found for both 4 and 6hours treated monoclinic WO_3 nanocuboids without significant effect of any crystalline water.

3.6. Electrochromic response of WO_3 nanocuboids

The optimized WO_3 nanocuboid coated onto ITO conducting substrate (WO_3/ITO) is used as the working electrode for electrochemical analysis. The fabricated dip-coated WO_3/ITO electrodes are semi-transparent in nature. The direct optical transmittance of the fabricated electrode has transparency of about 52%.In order to evaluate the electrochromic properties, typical cyclic voltammograms (CV)has been taken between -1.0 to +1.0V at a scan rate of 100mV/s using 1M H_2SO_4 as the working electrolyte. Figure 9a shows the cyclic voltammograms recorded for WO_3/ITO electrode at the 1st,

$100^{th}$and 500^{th} cycles. It can be seen that the shape of the CV curves remain unchanged after 100 and 500^{th}cycles with negligible increased current response, which indicates good cycling stability of the WO_3/ITO electrodes.This is probably due to the well distribution of the particles on the ITO surface after drying of the WO_3 nanocuboids dip-coated ITO electrodes. The topographical FESEM image shows the distribution and texture of particles on the ITO glass surface. It is evident from the image that the particles are relatively well distributed and interconnected. However, the small (~200nm) pin holes may provide additional ion transportation phenomenon and subsequent electrochromic behavior. The electrochromic mechanism of WO_3/ITO electrodes in H^+ electrolyte can be well expressed as follows:

$$WO_3 + xe^- + xH^+ \leftrightarrow H_xWO_3 \quad (4)$$

A unique coloration and bleaching processes have been observed for WO_3nanocuboidscoated ITOelectrodesduring the intercalation and deintercalation of electrons from the WO_3/ITO electrode and H^+ ions from the electrolyte. As shown in the CV curves, the current is found to move negatively with decreasing voltage, corresponding to that, co-intercalation of electrons and H^+ into WO_3 to form hydrogen tungsten bronzes takes place [23].Cathodic and anodic current peaks are observed near to-0.25Vand 0.1V, respectively. The current density observed for WO_3/ITO electrode is near to 3.15mA/cm^2. Most importantly, high symmetry of the anodic and cathodic peak is found which reveals the better electrochromic behavior of WO_3nanocuboids.A reversible color change of the WO_3/ITO electrodes with varying voltages has been observed. The initial WO_3/ITO electrode is light green in color but upon application of -0.5V, the electrode color changes to light blue which then further turns to darker blue at -1.0V. Bleaching of the electrode occurs at positive voltage of 0.5V and 1.0V, respectively. Thus we can conclude that, during the deintercalation of H^+ ions, the color of the electrodes bleach gradually with increasing voltage and finally the original color is recovered. This observation predicts that at positive voltage bleaching of the electrodes occur. The estimation of coloration and bleaching time for WO_3/ITO electrode is known from the current time transients. A

typical CA graph has been shown in Figure 10 for the coloration and bleaching of WO_3/ITO electrodes. During the measurement of CA, experimentally voltage is allowed to sweep from its rest potential of 0.0V to -1V for a period of 10seconds to obtain the coloration phenomenon of the electrodes. Similarly, in reverse, a positive voltage of 1V is applied for the next 10 seconds which results in bleaching of electrodes. An interesting coloration and bleaching kinetics is recorded from this analysis. Diffusion of H^+ to the electrolyte (bleaching process) is faster than the diffusion of H^+ from the electrolyte (coloration process) and hence needs 3.18 seconds and 5.05 seconds, respectively. The faster bleaching kinetics than the coloration kinetics is governed possibly by space charge transfer through the electrode and potential barrier at electrolyte - WO_3 interface respectively which controls the two processes diversely.

In order to study the amount of charge intercalation of e^- and H^+ ions from an electrolyte with respect to time, Chronocoulometry measurement of WO_3/ITO electrode is carried out at voltage sweep range between -1.0V to +1.0V. The CC measurement for intercalation and deintercalation process is carried out for the step of 10 seconds each for forward and backward scan. Figure 11 represents a typical CC plot of WO_3/ITO electrode for the first cycle and the inset figure represents the CC plot for first 15 cycles. During the forward scan of WO_3/ITO electrode, diffusion process leads to the charge intercalation by reducing W^{6+} to W^{5+} states. In the reverse, removal of intercalated charge occurs during the backward bleaching process due to oxidation of $W^{5+}$to W^{6+} states.The charge intercalation and deintercalation quantified data from the plot has been used to calculate the reversibility of the coloration/bleaching processes. The reversibility of the film can be calculated from the following relation mentioned below:

$$\text{Reversibility} = \frac{Q_{di}}{Q_i} \quad (5)$$

Where, Q_{di} and $Q_i$refers to the amount of charge deintercalated and intercalated in the WO_3/ITO films. The percentage electrochromic reversibility of the WO_3/ITO electrode for first cycle is ~72.2%. There is a slight increment in the reversibility after first CC cycle which remains almost constant till the 15th

cycle. The reversibility difference between 1st and 2nd cycle is approximately 5%. As from CV, the electrode exhibits high stability till 500th cycle, it is obvious to interpret that the reversibility also remains same.The UV-Visible transmittance spectroscopy is performed for WO_3/ITO electrodes in the wavelength range between 200 – 900nm after performing the electrochemical analysis. Figure 12 shows the room temperature optical transmittancedata for WO_3/ITO colored and WO_3/ITO bleached electrodes. The merit of optical performance is to quantify the optical density change (ΔOD) and the coloration efficiency of the WO_3/ITO films. The optical transmittance has been found to decrease with the coloration of the films and then increase upon the deintercalation process.The transmittancevalue of WO_3/ITO electrodes at visible wavelength of 550nm isutilized for determining the optical density changes. The ΔOD calculation is done as per the following relation given below [35]:

$$\Delta OD = log \frac{T_b}{T_c} \quad (6)$$

Where, T_b and T_c are the transmittance value in the bleached and colored state, respectively. The achieved transmittance efficiency for both bleached and colored monoclinic WO_3 thin film is well comparable with reported data [36]. The coloration and bleaching of WO_3/ITO electrodeis carried out by applying a potential step of -1.0V to +1.0V for a fixed time. One of the prime parameter to characterize an electrochromic material is coloration efficiency (CE) of the electrodes. In order to quantify the efficiency during the induction of charge in an electrochromic device, CE is represented as the change in optical density (ΔOD) per unit charge insertion per unit area. It is given by the following relation mentioned below:

$$CE = \frac{\Delta OD}{Q_i/A} \quad (7)$$

Where, Q_i is the amount of charge intercalated in WO_3/ITO electrodes to cause the change in optical density (ΔOD) and A is the area of the electrode. Thus, the coloration efficiency as calculated for WO_3/ITO electrode has been found to be 60.17cm^2/C. The result obtained is in accordance to reports by other groups[37, 38].

4. Conclusion

Initial variation of HBF_4 concentration at temperature 180°C and time 4hours follows triclinic WO_3 → hexagonal WO_3 → monoclinic WO_3 phase transformation to obtain WO_3 nanocuboids from sodium tungstate. On the other hand, monoclinic and cuboid tungsten trioxide develops through orthorhombic tungstite → monoclinic WO_3at an optimum fluoroboric acid concentration. Hydrothermal time, temperature and structure directing reagent concentration have significant influence to achieve phase and desire morphology. Nanocuboid exhibits an optimum band gap and adherence to develop dip-coated WO_3/ITO electrode. Tungsten trioxide coated ITO electrode has remarkable electrochemical response, electrochromic efficiency, reversibility, and optical switching characteristics. The developed process and achieved an electrochromic response is considerably appreciable, which might have economic viability to fabricate any tailor-made smart glass.

References:

[1] J. Ma, J. Zhang, S. Wang, T. Wang, J. Lian, X. Duan, W. Zheng, *J. Phys. Chem. C.*2011, 115, 18157.

[2] L. Liang, J. Zhang, Y. Zhou, J. Xie, X. Zhang, M. Guan, B. Pan, Y. Xie, *Scientific Reports*, 2013, 3, 1936.

[3] X. He, C. Hu, Q. Yi, X. Wang, H. Hua, X. Li,*Catal. Lett*.,2012, 142, 637.

[4] S. Vallejos, T. Stoycheva, P. Umek, C. Navio, R. Synders, C. Bittencourt, E. Llobet, C. Blackman, S. Moniz, X. Correig,*Chem. Comm*., 2011, 47, 565.

[5] B.X. Li, G. X. Rong, Y.Xie, L.F. Huang, C. Q. Feng, *Inorg. Chem*., 2006, 45,6404.

[6] Q. Sun, J. Luo, Z. Xie, J. Wang, X. Su, *Mater. Lett*.,2008, 62,2992.

[7] A. Wolcott, T. R. Kuykendall, W. Chen, S. Chen, J. Z. Zhang, *J. Phys. Chem. B*,2006, 110, 25288.

[8] Z. Zhao and M. Miyauchi, *J. Phys. Chem. C*,2009,113, 6539.

[9] Y. H. Jun, C. Y. Qi, Y. Fang, P. Y. Hua, H. X. Wu, Z.Ding, T. D. Sheng,*Chin. Phys. B*,2011, 20,036103.

[10]B. Yang, P. R. F. Barnes, Y. Zhang, V. Luca, *Catal. Lett.*, 2007, 118, 280.

[11] H. Hassani, E. Marzbanrad, C. Zamani, B. Raissi, *J. Mater. Sci.: Mater. Electron*, 2011, 22, 1264.

[12] A. Novinrooz, M. Sharbatdaran, H. Noorkojouri, *Cent. European J. Phys*., 2005, 3[3], 456.

[13] X. Song, Y. Zhao, Y. Zheng,*Mater. Lett*.,2006, 60, 3405.

[14] S. Rajagopal, D. Nataraj, D. Mangalaraj, Y. Djaoued, J. Robichand, O. Y. Khyzhun,*Nanoscale Res. Lett.*, 2009, 4, 1335.

[15] X. Su, F. Xiao, Y. Li, J. Jian, Q. Sun, J. Wang, *Mater. Lett*., 2010, 64, 1232.

[16] Y. Choi, G. Sakai, K. Shimanoe, N. Miura, N. Yamazoe, *Sensors and Actuators B*, 2003, 95, 258.

[17] M. G. Fabra, P. Dunne, D. Grant, P. Gooden, E. Lester, *Chem. Engg. J*., 2013,226, 22.

[18] Z. Jiao, X. Wang, J. Wang, L. Ke, H. V. Demir, T. W. Koh, X. W. Sun, *Chem. Comm*., 2012, 48,365.

[19] Z. Jiao, J. Wang, L. Ke, X. W. Sun, H. V. Demir, *Appl. Mater. Interfaces*, 2011, 3, 229.

[20] G. Leftheriotis, S. Papaefthimiou, P. Yianoulis, A. Siokou, D. Kefalas, *Appl. Surf. Sci*.,2003, 218, 275.

[21] Z. Jiao, X. W. Sun, J. Wang, L. Ke, H. V. Demir, J. Phys. D: Appl. Phys., 2010, 43, 285501.

[22] G. Xin, W. Guo, T. Ma, *Appl. Surface Sci*., 2009, 256, 165.

[23] X. Chang, S. Sun, Z. Li, X. Xu, Y. Qui, *Appl. Surface Sci*., 2011,257, 5726.

[24] D. S. Hinczewski, M. Hinczewski, I. Sorar, F. Z. Tepehan, G. G.Tepehan, *Sol. Energy Mat*., 2008, 92, 821.

[25] N. M. G. Parreira, N. J. M. Carvalho, A. Cavaleiro, *Thin Solid Films*, 2006, 510, 191.

[26] J. K. Kim, K. Shin, S. M. Cho, T. Lee, J. H. Park, *Energy Environ. Sci*., 2011, 4, 1465.

[27] H. Zheng, J. Ou, M. S. Strano, R. B. Kaner, A. Mitchell, K. K. Zadeh, *Adv. Func. Mater.,*2011, 21, 2175.

[28] I. M. Szilagyi, L. Wang, P. Gouma, C. Balazsi, J. Madarasz, G. Pokol, *Mater. Res. Bull*., 2009, 44, 505.

[29] D. Sarkar, M. Chu, S. Cho, Y. Kim, B. Basu, *J. Am. Ceram. Soc*.,2009, 92,2877.

[30] P. Reiss, M. Protiere, L. Li, *Small*, 2009, 5, 154.

[31] S. Pokhrel, J. Birkenstock, M. Schowalter, A. Rosenauer, L. Madler, *Cryt. Growth & Design*, 2010, 10, 632.

[32] F. Huang, H. Zhang, J. F. Banfield, *Nano Letters*,2003, 3, 373.

[33] H. Hayashi, Y. Hakuta, *Materials*, 2010, 3, 3794.

[34] D. Chen, H. Wang, R. Zhang, L. Gao, Y. Sugahara, A. Yasumori, *J. Cer. Processing*, 2008, 9, 596.

[35] D. S. Dalavi, R. S. Devan, R. A. Patil, R. S. Patil, Y. R. Ma, S. B. Sadale, I. Y. Kim, J. H. Kim, P. S. Patil, *J. Mater. Chem*., 2013, 1, 3722.

[36] C. K. Wang, C. K. Lin, C. L. Wu, S. C. Wang, J. L. Huang, *Electrochim. Acta,,* 2013, 112, 24.

[37] F. Lin, J. Cheng, C. Engtrakul, A. C. Dillon, D. Nordlund, R. G. Moore, T. C. Weng, S. K. R. Williams, R. M. Richards, *J. Mater. Chem*., 2012, 22, 16817.

[38] M. Deepa, R. Sharma, A. Basu, S. A. Agnihotry, *Electrochim. Acta*, 2005, 50, 3545.

Figure Captions:

Figure 1: XRD patterns for the effect of HBF_4 molar concentration at 180^oC for -4hours (a), Effect of time at 180^oC with 4M HBF_4 concentration (b) andeffect of temperature for 6hours at 4M HBF_4 concentration (c);where, *=triclinic; # =monoclinic; ^ = hexagonal; @=orthorhombic tungstite crystal structure.

Figure 2: Rietveld Refinement of WO_3Nanocuboids; prepared at 180^oC, 6hours and 4M HBF_4.

Figure 3: TG-DSC plot of WO_3nanocuboids a) 4hours and b) 6hours

Figure 4: FESEM images under experimental conditions of time 6hours and temperature 180^oC at: (a) 3.5M, (b) 4M and (c) 4.5M HBF_4 concentrations.

Figure 5: FESEM images under experimental conditions of 4M HBF_4 concentration and temperature 180^oC for: (a) 2hours, (b) 4hours, (c) 6hours and (d) 8hours time duration and (e) BET surface area vs. time plot.

Figure 6: FESEM images under experimental conditions of 4M HBF_4 concentration for time 6hours at: (a) 170^oC and (b) 190^oC of temperature.

Figure 7: TEM analysis of WO_3nanocuboids; a) Morphology, b) d-spacing and c) SAED pattern

Figure 8: UV-DRS of 2M HBF_4, 3M HBF_4, 4hours and 6hours. Inset represents the Tauc Plot.

Figure 9: (a) Cyclic Voltammograms of WO_3/ITO film at 100mV/s for 1st, 100th and 500th cycle. (b) Topographical image of dip coated WO_3 nanocuboids onto ITO glass substrate.

Figure 10: Chronoamperometry (CA) measurement for WO_3/ITO film.

Figure 11: Chronocoulometry (CC) measurement for WO_3/ITO film.(Inset represents the CC for first 15cycles).

Figure 12: Optical transmittance spectra versus wavelength of colored and bleached films.

List of Figures:

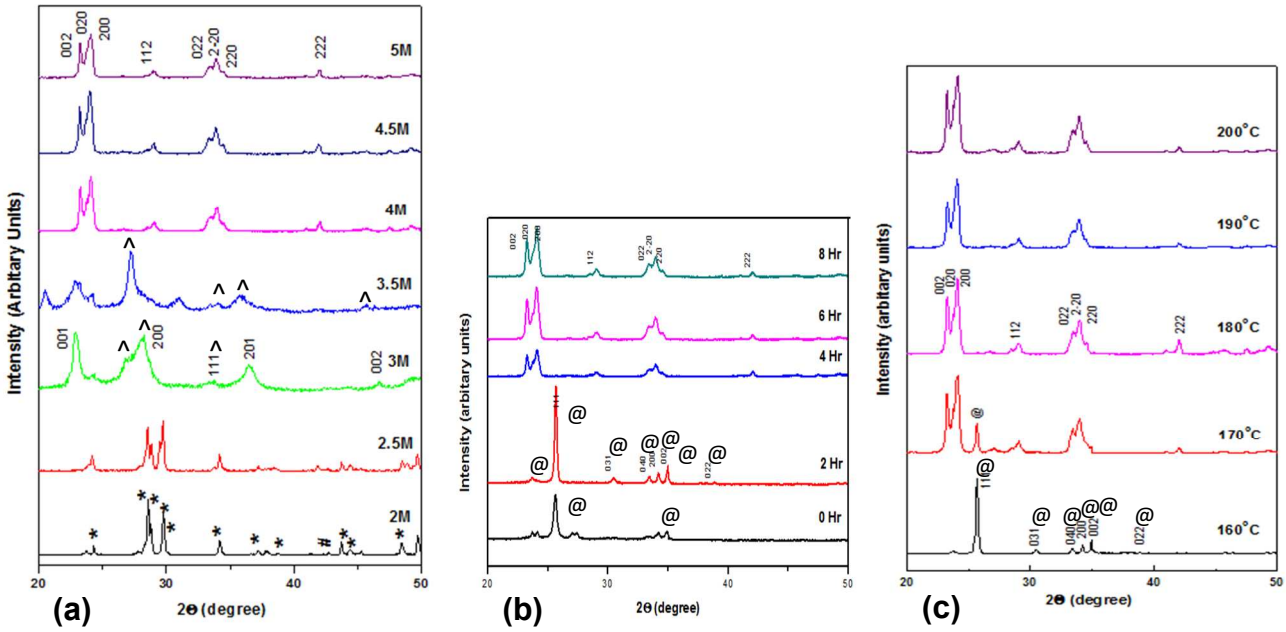

Figure 1

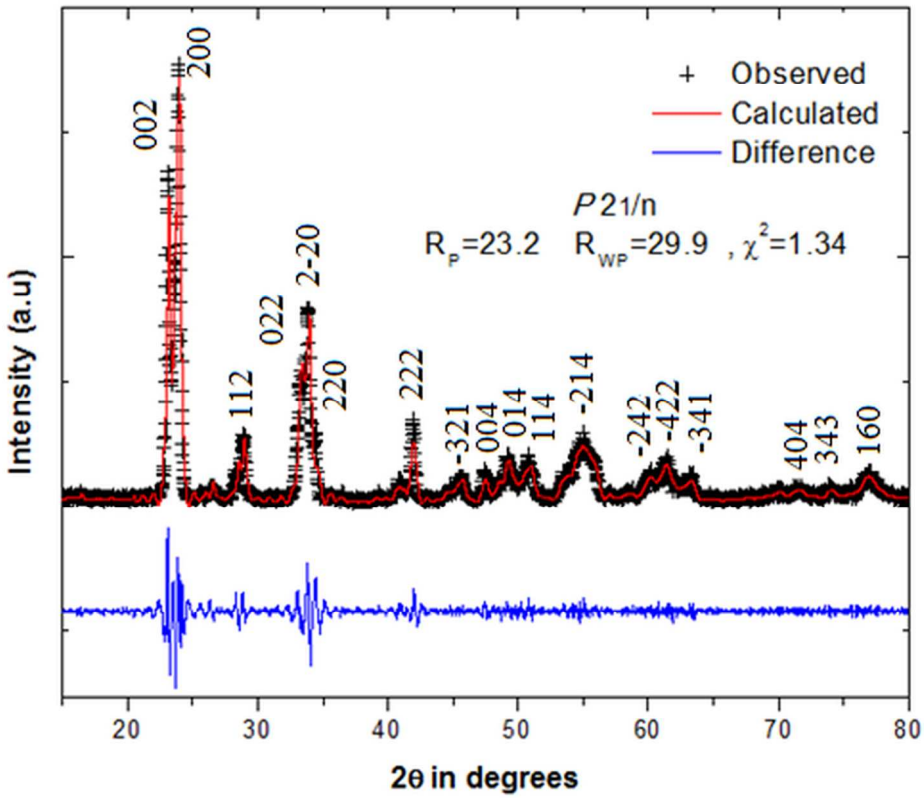

Figure 2

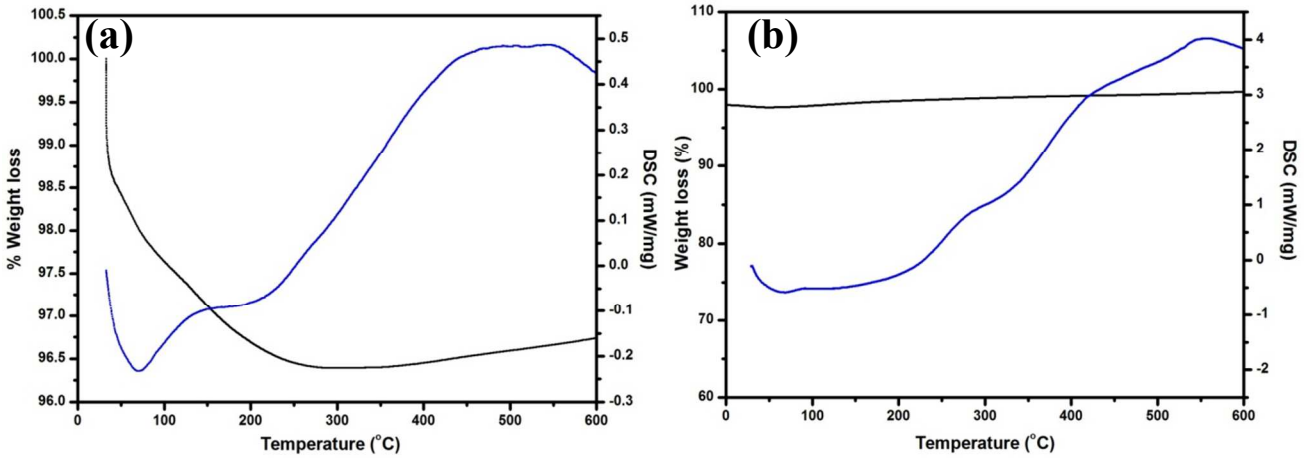

Figure 3

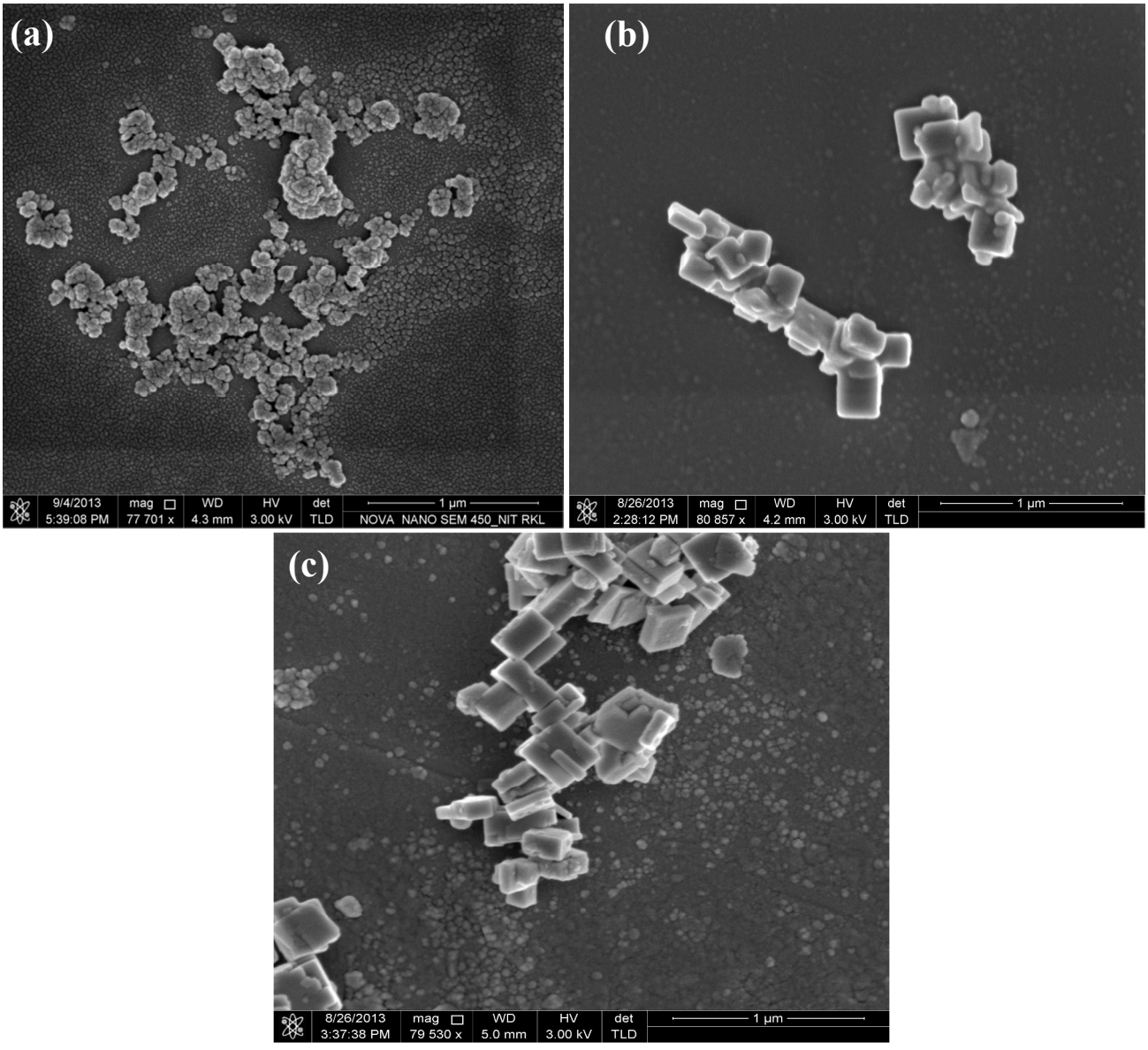

Figure4

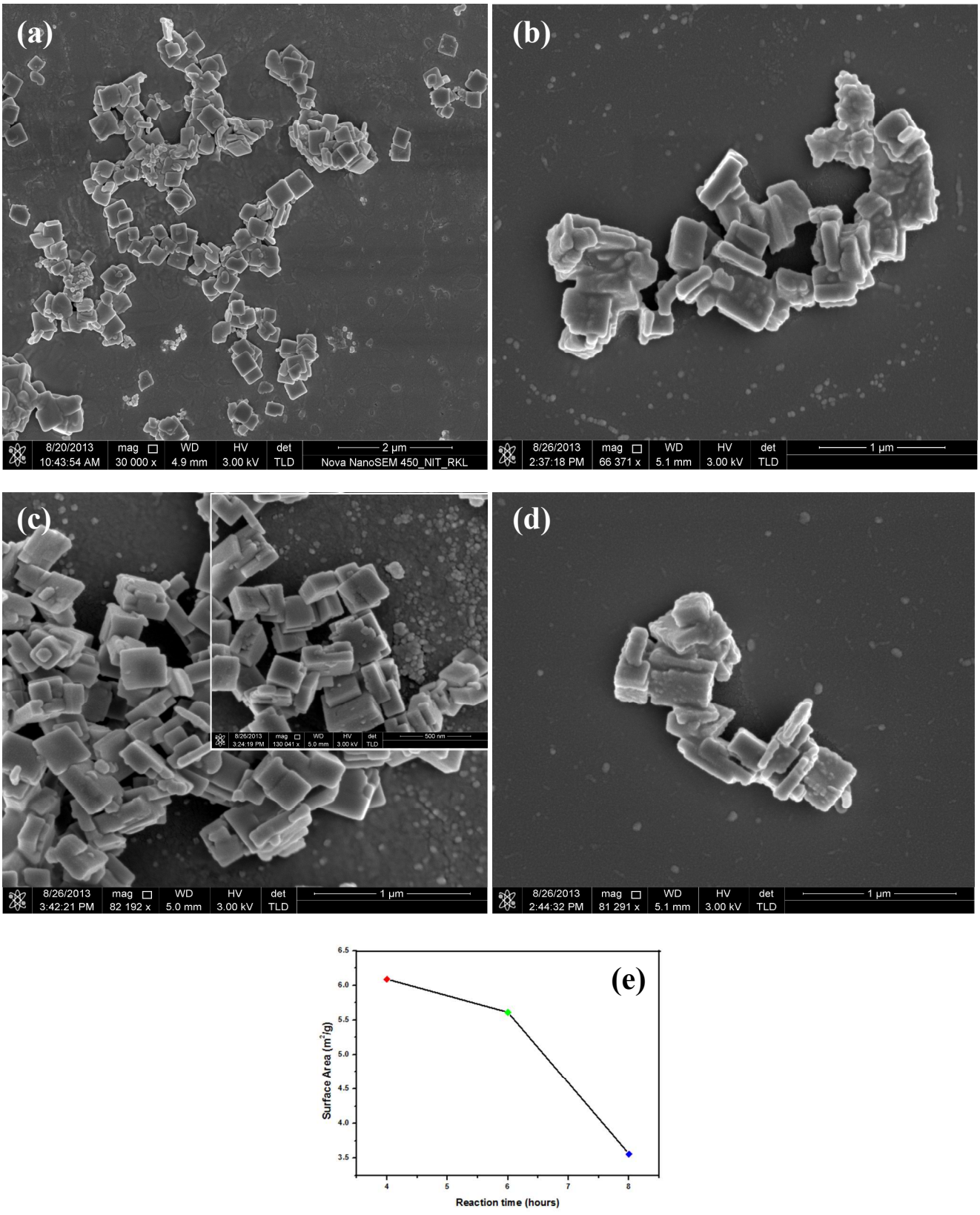

Figure 5

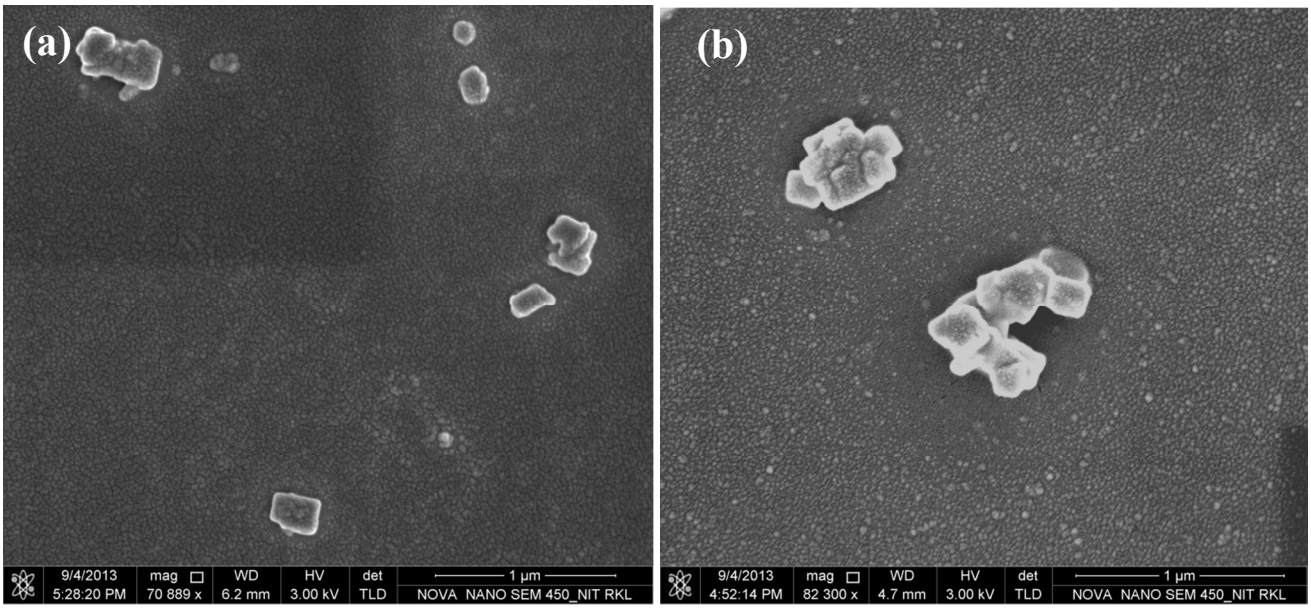

Figure 6

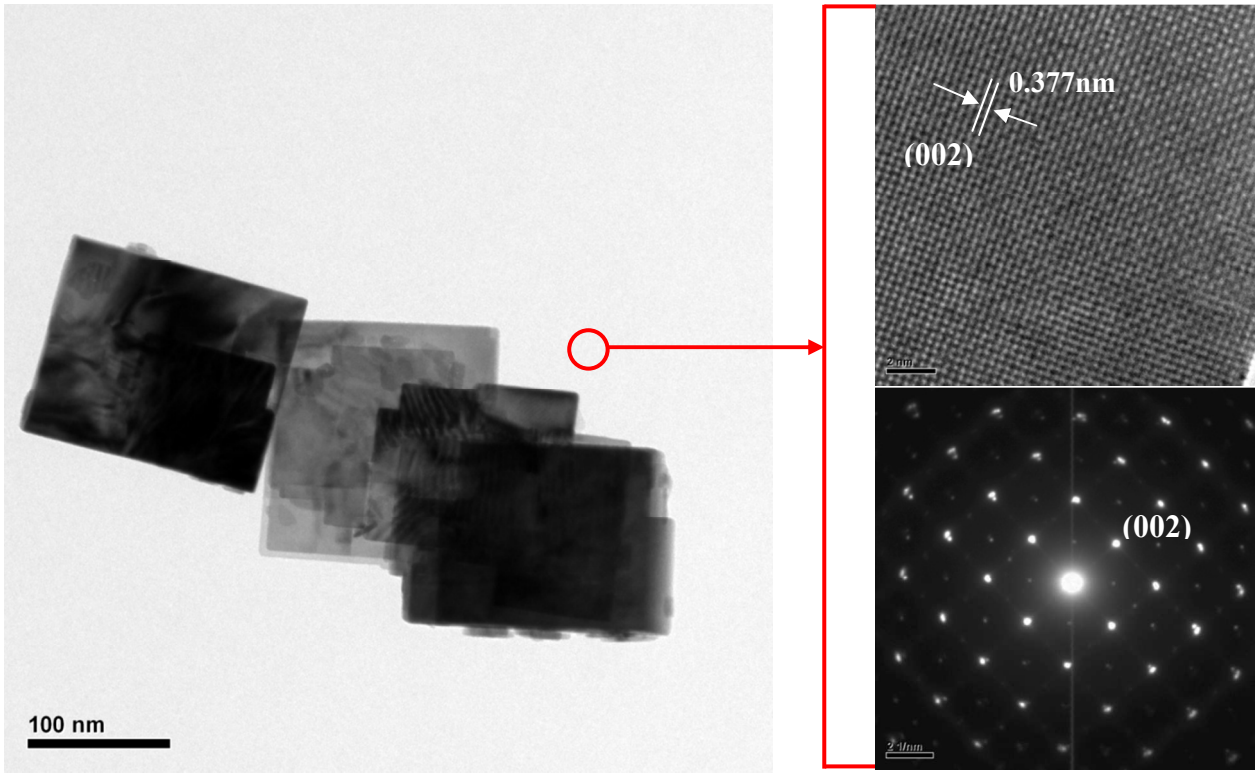

Figure 7

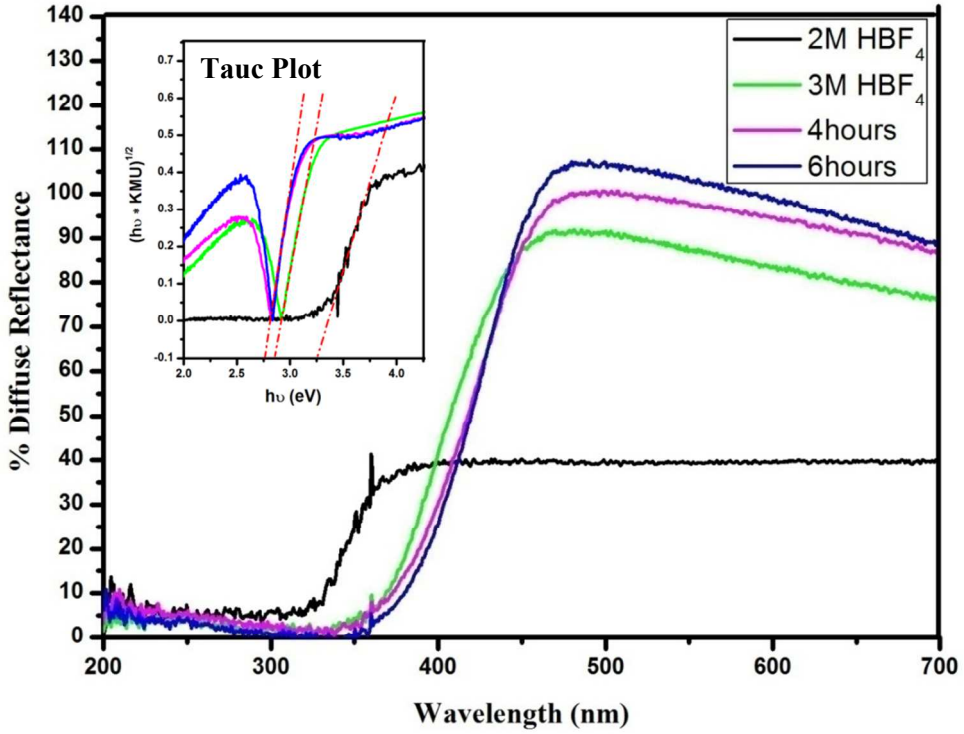

Figure 8

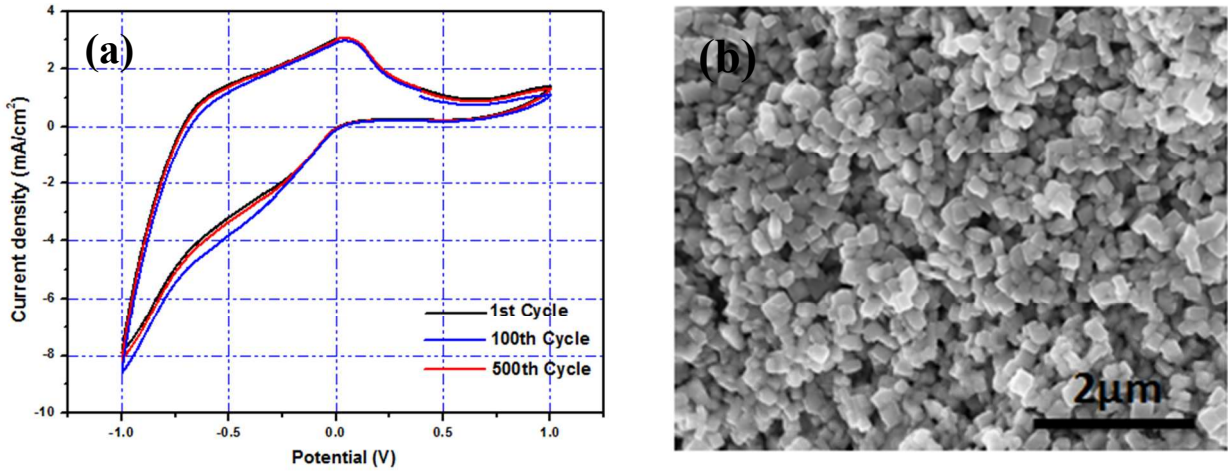

Figure 9

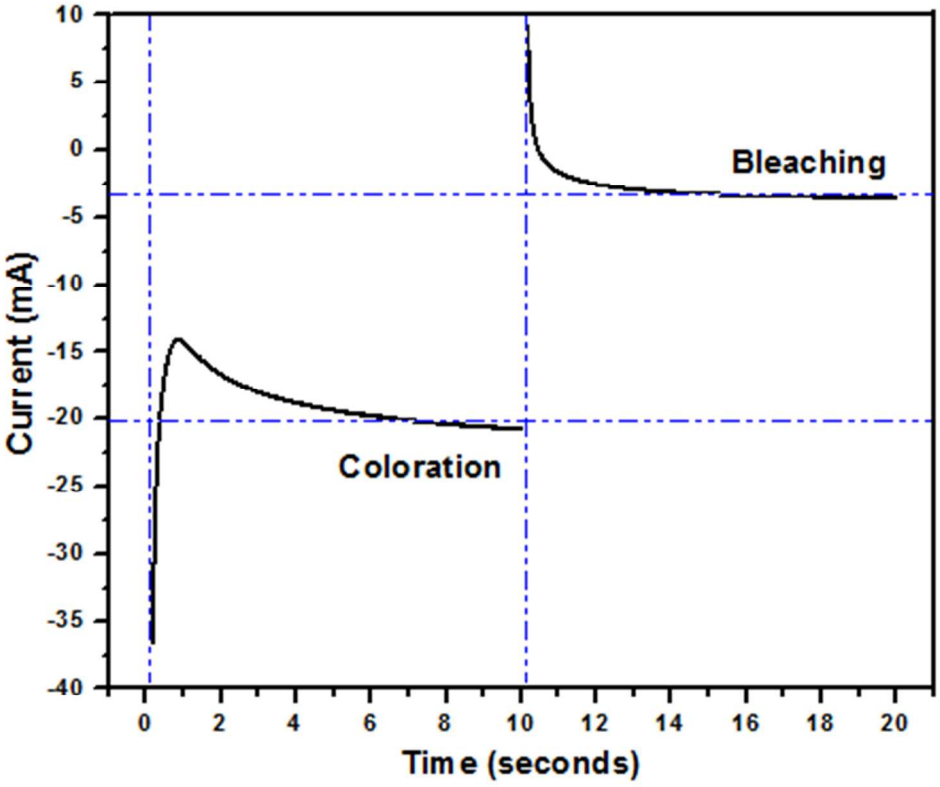

Figure 10

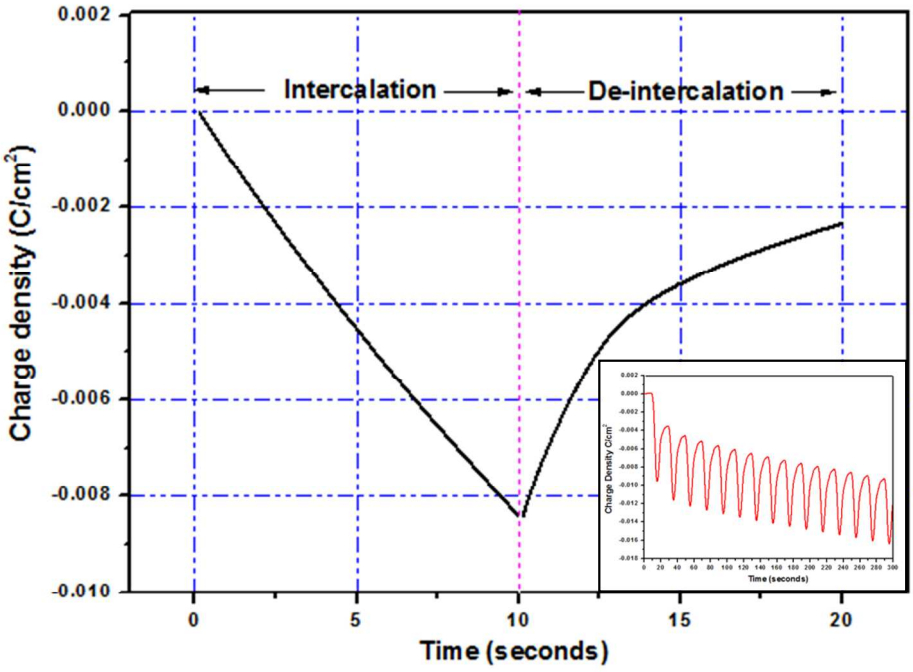

Figure 11

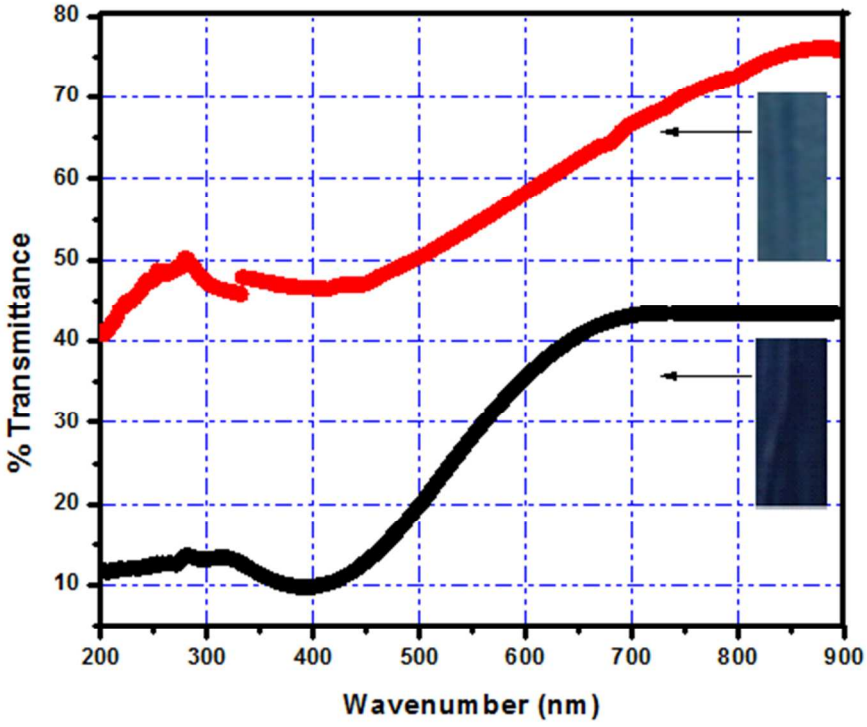

Figure 12